

Synthesis of high-entropy-alloy-type superconductors (Fe,Co,Ni,Rh,Ir)Zr₂ with tunable transition temperature

Md. Riad Kasem¹, Aichi Yamashita¹, Yosuke Goto¹, Tatsuma D. Matsuda¹, Yoshikazu Mizuguchi^{1*}

1. Department of Physics, Tokyo Metropolitan University, 1-1, Minami-osawa, Hachioji, 192-0397.

(Corresponding author: mizugu@tmu.ac.jp)

KEYWORDS: New superconductors, High-entropy-alloy-type superconductor, $TrZr_2$, Tunable T_c

Abstract

We report on the synthesis and superconductivity of high-entropy-alloy-type (HEA-type) compounds $TrZr_2$ ($Tr = Fe, Co, Ni, Rh, Ir$), in which the Tr site satisfies the criterion of HEA. Polycrystalline samples of HEA-type $TrZr_2$ with four different compositions at the Tr site were synthesized by arc melting method. The phase purity and crystal structure were examined by Rietveld refinement of X-ray diffraction profile. It has been confirmed that the obtained samples have a $CuAl_2$ -type tetragonal structure. From analyses of elemental composition and mixing entropy at the Tr site, the HEA state for the Tr site was confirmed. The physical properties of obtained samples were characterized by electrical resistivity and magnetization measurements. All the samples show bulk superconductivity with various transition temperature (T_c). The T_c varied according to the compositions and showed correlations with the lattice constant c and Tr -Zr bond lengths. Introduction of an HEA site in $TrZr_2$ is useful to achieve systematic tuning of T_c with a wide temperature range, which would be a merit for superconductivity application.

1. Introduction

Superconductivity is a macroscopic quantum phenomenon typically characterized by zero-resistivity state, Meissner effect, and Josephson effects. Superconductors are used in large-scale application and device applications [1]. Particularly, low-transition temperature (low- T_c) metals and alloy, which is mostly Nb or Pb-based alloys, are used for device components like Josephson junctions. Since superconducting devices have been expected to be used in various purposes and scales in near future, development of new superconducting materials, which are easy to use in practical application and have tunable superconducting properties, are needed. In this study, to develop new superconducting materials system having tunability of T_c , we focus on high-entropy-alloy-type (HEA-type) compounds.

Recently, superconductivity in HEAs have been getting attention due to the possible robustness of superconducting states under extreme conditions and flexible tuning of superconducting properties by alloying [2-11], since the discovery of a $\text{Ta}_{34}\text{Nb}_{33}\text{Hf}_8\text{Zr}_{15}\text{Ti}_{11}$ superconductor with $T_c = 7.3$ K [2]. HEAs are typically defined as alloys composed of five or more elements with a concentration range between 5 to 35at%. Due to extremely high performance as high-temperature materials, structural materials, medical materials, etc., which are most probably resulted from high configurational mixing entropy (ΔS_{mix}) defined as $\Delta S_{\text{mix}} = -R \sum_i c_i \ln c_i$, where c_i and R are compositional ratio and the gas constant, HEAs have been extensively studied in the field of material science, engineering, chemistry and physics [12,13].

To further extend the field of HEA superconductors, we have synthesized HEA-type compounds, in which the crystal structure possesses an HEA-type site [14-18]. In addition, by Fujita et al., single crystals of $RE(\text{O},\text{F})\text{BiS}_2$ layered superconductors with an HEA-type rare-earth (RE) site were grown [19]. Although the number of the examples of HEA-type superconductors is still limited, various (positive or negative) effect of increased mixing entropy (ΔS_{mix}) to the superconducting characteristics have been observed [14,17,20]. Very recently, we reported the synthesis of $\text{Co}_{0.2}\text{Ni}_{0.1}\text{Cu}_{0.1}\text{Rh}_{0.3}\text{Ir}_{0.3}\text{Zr}_2$ and the emergence of bulk superconductivity with $T_c = 8$ K [21]. This material has a tetragonal CuAl_2 -type structure ($I4/mcm$, #140) and is a member of $Tr\text{Zr}_2$ (Tr : transition metal). $Tr\text{Zr}_2$ has been studied as

superconducting system with a relatively high T_c up to 11.3 K for $Tr = \text{Rh}$ [22-24] and as hydrogen-storage materials [25]. The T_c of those $Tr\text{Zr}_2$ varies largely by element substitution: $T_c = 0.17, 5.5, 1.6, 11.3, 7.5$ K for $Tr = \text{Fe}, \text{Co}, \text{Ni}, \text{Rh}, \text{and Ir}$, respectively. On the basis of the fact, we considered that the $Tr\text{Zr}_2$ system is suitable for T_c tuning with a wide temperature range. In this study, we choose $Tr = \text{Fe}, \text{Ni}, \text{Co}, \text{Rh}, \text{and Ir}$ because pure $Tr\text{Zr}_2$ compounds with those Tr elements show superconductivity as mentioned above. We have synthesized four HEA-type $(\text{Fe}, \text{Co}, \text{Ni}, \text{Rh}, \text{Ir})\text{Zr}_2$ polycrystalline samples and observed bulk superconductivity with variable T_c by changing the Tr -site compositions.

2. Materials and methods

Polycrystalline samples of $Tr\text{Zr}_2$ with $Tr = (\text{A}) \text{Fe}_{0.1}\text{Co}_{0.2}\text{Ni}_{0.1}\text{Rh}_{0.3}\text{Ir}_{0.3}$, $(\text{B}) \text{Fe}_{0.1}\text{Co}_{0.3}\text{Ni}_{0.2}\text{Rh}_{0.1}\text{Ir}_{0.3}$, $(\text{C}) \text{Fe}_{0.2}\text{Co}_{0.2}\text{Ni}_{0.2}\text{Rh}_{0.2}\text{Ir}_{0.2}$, and $(\text{D}) \text{Fe}_{0.3}\text{Co}_{0.2}\text{Ni}_{0.3}\text{Rh}_{0.1}\text{Ir}_{0.1}$ were synthesized by arc melting in Ar atmosphere. Powders of pure Co (99%), Ni (99.9%), Fe (99.9%), Rh (99.9%), and Ir (99.9%), were mixed with a certain composition by mortar and pestle and pelletized into 7mm in diameter. The metal pellet and plates of pure Zr (99.2%) were used as starting materials. To obtain homogeneous sample, arc melting was repeated five times for all the samples. The weight (typically 1 g in total) loss was less than 1 % for all samples. The chemical compositions of the obtained samples were characterized by energy dispersive X-ray fluorescence analysis with a spot size of 0.9 mm on JSX-1000S (JEOL). The phase purity and the crystal structure were examined by powder X-ray diffraction (XRD) with Cu-K α radiation by the θ -2 θ method on Miniflex-600 (RIGAKU) equipped with a high-resolution semiconductor detector D/tex-Ultra. The obtained XRD patterns were refined by the Rietveld method using RIETAN-FP [26], and schematic images of the refined crystal structure were depicted using VESTA [27]. Electrical resistivity was measured by the four-probe method with a current of 5 A on a GM refrigerator system (AXIS). Magnetization measurements were performed by a superconducting quantum interference device (SQUID) on MPMS-3 (Quantum Design) under a magnetic field of 1 mT. The magnetic T_c was estimated as a temperature where magnetization clearly begins to decrease due to the emergence of diamagnetism. Irreversibility temperature (T_{irr}), which indicates the

emergence of superconducting current, was estimated as the temperature where the zero-field cooling (ZFC) data deviates from field cooling (FC) data. See Supporting Information (Fig. S1) for estimations of T_c and T_{irr} .

3. Results

The analyzed compositions and estimated ΔS_{mix} (Tr site) are listed in Table I. Since the actual compositions for the Tr site are close to starting nominal ones, we use starting nominal composition when displaying the results for the samples in this paper. Examined samples are labeled (A)–(D) according to the nominal compositions described in the synthesis part. In addition, the compositional ratio of all the constituent Tr -site elements for all the samples satisfy the criterion of HEA, which is 5 to 35 at%, and the estimated mixing entropy ΔS_{mix} (Tr site) is $1.50R$, $1.48R$, $1.61R$, and $1.52R$ for sample (A), (B), (C), and (D), respectively.

Figure 1(a) shows the powder XRD patterns for the obtained $TrZr_2$ samples. Tiny impurity peaks for cubic $IrZr_2$ (space group: No. 227) were observed. The main peaks of the XRD patterns were indexed by the tetragonal $CuAl_2$ -type structure (space group: $I4/mcm$). As shown in Fig. 1(b), the XRD peaks shift to higher angles from (A) to (D), which indicates that lattice constants decrease by decreasing average ionic radius of Tr . Figure 2 shows the results of the Rietveld refinements for sample (A)–(D). The reliability factor of the Rietveld refinement (R_{wp}) in a single-phase analysis was 6.2%, 5.6%, 4.6%, and 3.9% for sample (A), (B), (C), and (D), respectively. Those low R_{wp} support the synthesis of high-purity polycrystalline samples by arc melting and the appropriateness of the $CuAl_2$ -type structural model. The structural parameters obtained from the Rietveld analyses are summarized in Table II. Figure 1(c) displays schematic images of the refined crystal structure for sample (C) $Fe_{0.2}Co_{0.2}Ni_{0.2}Rh_{0.2}Ir_{0.2}Zr_2$, in which the Tr site is occupied by five transition metals. Three Zr-Zr bonds and two Tr -Zr bonds were defined as shown in the images.

Figure 3 shows the temperature dependences of electrical resistivity for sample (A)–(D). As shown in Fig. 3(a), zero resistivity was observed at $T_c^{zero} = 6.8, 5.7, 4.9, 3.9$ K for sample (A), (B), (C), and (D), respectively. As displayed in Fig. 3(b), all the samples show

the metallic temperature dependence of resistivity. The large residual resistivity ratio was observed for all the sample, which is a common trend seen in several HEA-type superconductors [2,16-18,21].

Figure 4 shows the temperature dependences of magnetization for sample (A)–(D). All the samples showed large diamagnetic signals. The observed ZFC and FC data show features of a typical type-II superconductor. The ZFC magnetization at 2 K for all the samples exceed a value expected from full shielding volume fraction. Therefore, the superconducting transition observed for all the samples are bulk in nature. Magnetic T_c^M and T_{irr} differs for those four samples: $T_c^M = 7.8, 6.7, 5.4$, and 4.8 (K) and $T_{irr} = 7.0, 5.9, 5.1$, and 4.2 K for sample (A), (B), (C), and (D). The T_c s estimated from resistivity and magnetization are comparable and show variation according to the composition at the *Tr* site.

4. Discussion

One of the notable trends of this system is that the observed T_c s for sample (A)–(D) are close to the *Tr-weighted-average* T_c of pure systems. Since introduction of disorders of the transition metal site sometimes largely affects superconducting properties of transition-metal-based compounds like Fe-based superconductors [26,27], the simple averaging effect on T_c is interesting. Since all the samples show bulk superconductivity, we propose that systematic tuning of T_c can be easily achieved in the *Tr*Zr₂ system. Such system would be useful for device application containing superconductors. As found in XRD analyses, the lattice constants continuously change according to the ionic radius of elements included in the structure. To obtain information about the relationship between T_c and structural parameters, T_c^M for various *Tr*Zr₂ are plotted in Figs. 5(a) and 5(b) as functions of lattice constants a and c . Those figures contain data points for non-HEA (pure) and related *Tr*Zr₂.

The lattice constant- a dependence of T_c (Fig. 5(a)) shows monotonous increase in T_c with increasing a for the present HEA-type samples (A)–(D). However, other data points do not show a significant correlation between T_c and a . In contrast, the lattice constant c shows a clear correlation with T_c (Fig. 5(b)). Actually, the *Tr*-Zr bonds (Table II) are expanded by increasing concentration of larger *Tr* such as Rh and Ir, while the Zr-Zr bond length does not show a remarkable dependence on the change in *Tr*-site concentration. Since the electronic

bands near the Fermi energy (E_F), which is essential for the superconductivity, are contributed by both Zr- d and Tr - d electrons [24], the systematic change in bonding states along the c -axis, which is mainly composed of Tr -Zr bonds, may systematically tunes density of states at the E_F and hence T_c in the $TrZr_2$ system. We note that the data point for $FeZr_2$ does not obey the relation proposed above. In Ref. 32, the presence of weak ferromagnetism was reported for $FeZr_2$. The presence of magnetism may be related to the low T_c for $FeZr_2$. Although our HEA-type samples contain Fe with various concentration (about 30% for (D)), the presence of Fe does not affect the relation; sample (D) also obeys the trend. The random solution in the HEA-type compounds may be effective to the suppression of magnetic ordering. If the assumption is correct, this fact should positively work on systematic tuning of T_c by compositional manipulation in HEA-type $TrZr_2$. To obtain further knowledge, synchrotron XRD experiments and/or experiments sensitive to local structure, such as X-ray absorption spectroscopy, are needed for the system.

5. Conclusion

We have synthesized polycrystalline samples of new HEA-type $TrZr_2$ superconductors with $Tr = Fe, Co, Ni, Rh, \text{ and } Ir$ by arc melting. By Rietveld refinements of the powder XRD patterns, the crystal structures were confirmed to belong to the $CuAl_2$ -type tetragonal structure. All the samples show bulk superconductivity with various T_c . The T_c shows a correlation with lattice constant c and Tr -Zr bond length along the c -axis. This can be related to the electronic states contributed by both Tr - d and Zr - d electrons near the E_F in $TrZr_2$. We propose that HEA effects are useful to achieve systematic tuning of T_c with a wide temperature range in $TrZr_2$, which is possibly due to the systematic tuning of density of states at E_F and suppression of magnetism in high-entropy alloying. Such trend (functionality) would be useful for device application containing superconductors.

Acknowledgements

The authors thank O. Miura for their assistance with the experiments. This work was partly supported by JSPS KAKENHI (Grant Number: 18KK0076) and Tokyo Metropolitan Government Advanced Research (Grant Number: H31-1).

Table I. Actual composition (XRF) and estimated ΔS_{mix} (*Tr* site) for the examined *TrZr*₂ samples (A)–(D).

Label	Actual <i>Tr</i> composition (XRF)	ΔS_{mix} (<i>Tr</i> site)
(A)	Fe _{0.093} Co _{0.194} Ni _{0.113} Rh _{0.271} Ir _{0.329}	1.50 <i>R</i>
(B)	Fe _{0.108} Co _{0.297} Ni _{0.202} Rh _{0.073} Ir _{0.320}	1.48 <i>R</i>
(C)	Fe _{0.190} Co _{0.190} Ni _{0.200} Rh _{0.212} Ir _{0.208}	1.61 <i>R</i>
(D)	Fe _{0.293} Co _{0.190} Ni _{0.300} Rh _{0.093} Ir _{0.124}	1.52 <i>R</i>

Table II. Structural data and T_c for the *TrZr*₂ samples.

Label	(A)	(B)	(C)	(D)
Space group	<i>I4/mcm</i>			
<i>a</i> (Å)	6.4711(3)	6.4671(4)	6.4517(2)	6.4406(3)
<i>c</i> (Å)	5.5621(3)	5.5287(4)	5.5226(2)	5.4825(3)
V (Å ³)	232.91(2)	231.23(3)	229.87(2)	227.42(2)
x (Zr)	0.1673(3)	0.1682(3)	0.1683(2)	0.1696(2)
y (Zr)	0.6679(3)	0.6689(3)	0.6670(2)	0.6690(2)
<i>R</i> _{wp} (%)	6.2	5.6	4.6	3.9
Zr-Zr 1 (Å)	3.4056(13)	3.3994(13)	3.3990(9)	3.3827(9)
Zr-Zr 2 (Å)	3.411(3)	3.4022(13)	3.404(2)	3.388(2)
Zr-Zr 3 (Å)	3.164(2)	3.140(2)	3.1437(13)	3.1106(13)
Tr-Zr 1 (Å)	2.779(2)	2.771(2)	2.7653(12)	2.7553(12)
Tr-Zr 2 (Å)	2.784(2)	2.776(2)	2.7750(12)	2.7598(12)
T_c^{zero} (K)	6.8	5.7	4.9	3.9
T_c^M (K)	7.8	6.7	5.4	4.8
T_{irr} (K)	7.0	5.9	5.1	4.2

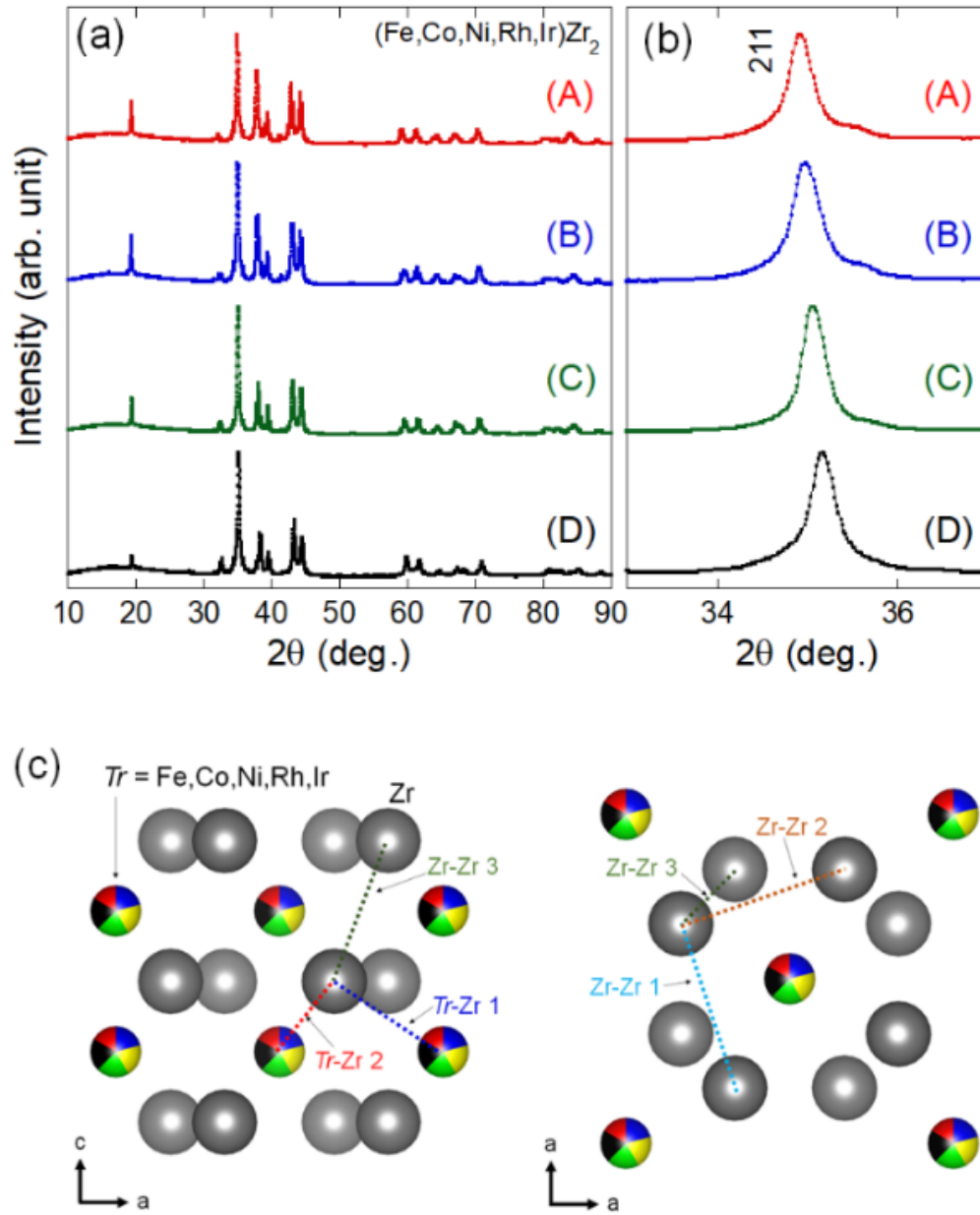


Fig. 1. (a) Powder XRD patterns for the obtained TrZr_2 samples (A)–(D). (b) Zoomed profiles near the 211 peak. (c) Schematic images of the crystal structure of sample (C) $\text{Fe}_{0.2}\text{Co}_{0.2}\text{Ni}_{0.2}\text{Rh}_{0.2}\text{Ir}_{0.2}\text{Zr}_2$.

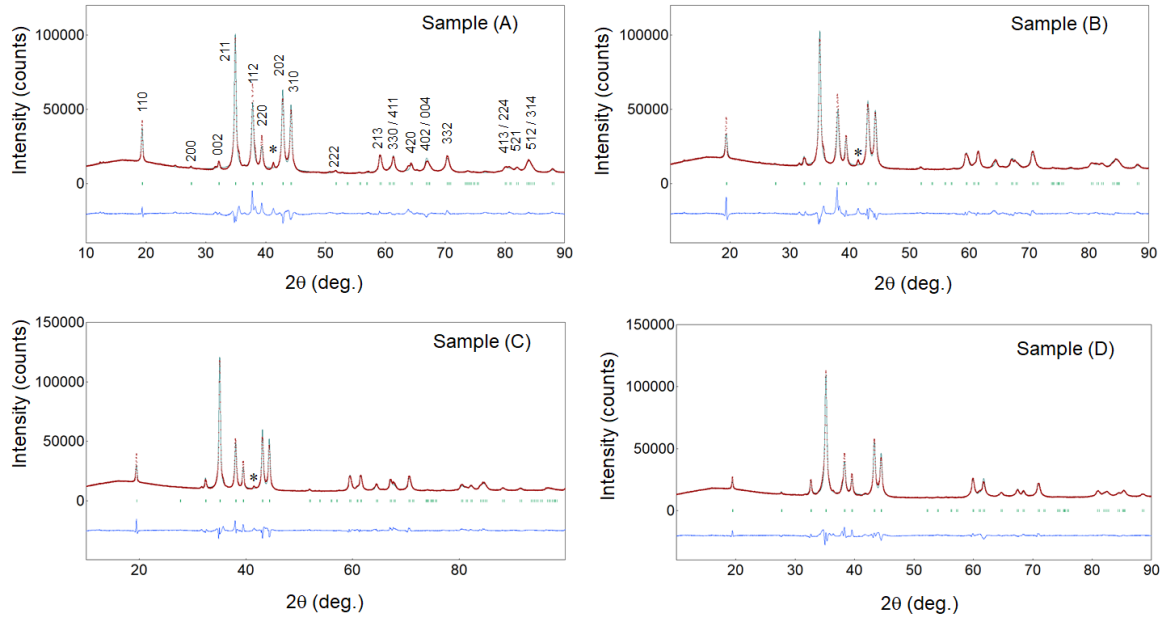


Fig. 2. (a) Powder XRD patterns for the obtained $TrZr_2$ samples (A)–(D). (b) Zoomed profiles near the 211 peak. (c) Schematic images of the crystal structure of sample (C) $Fe_{0.2}Co_{0.2}Ni_{0.2}Rh_{0.2}Ir_{0.2}Zr_2$.

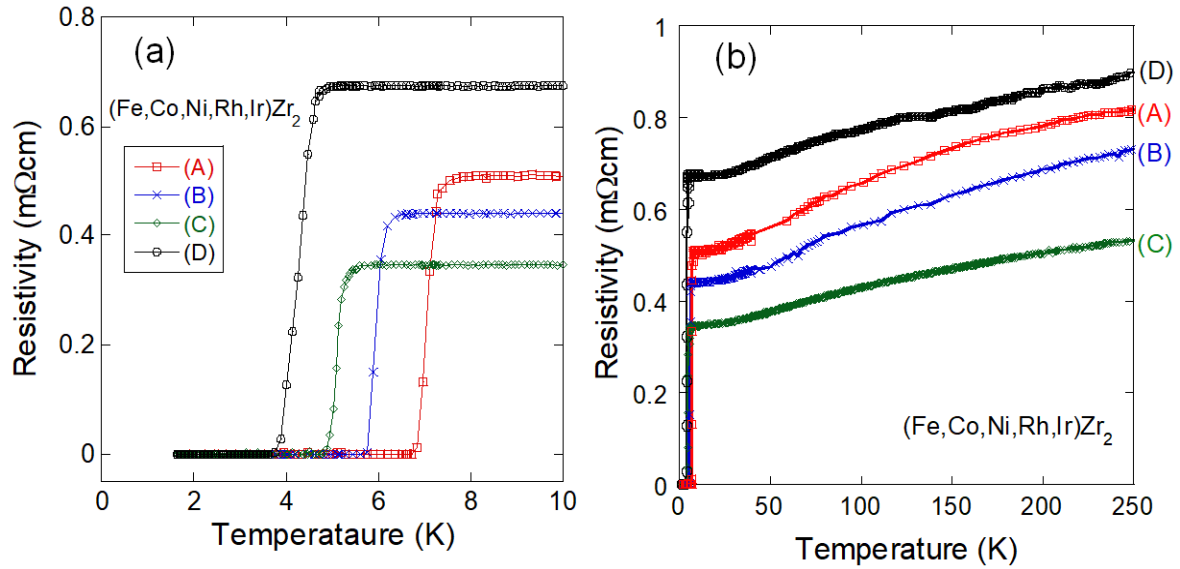


Fig. 3. Temperature dependences of electrical resistivity for $TrZr_2$ samples (A)–(D) at low temperatures (a) and whole temperature range (b).

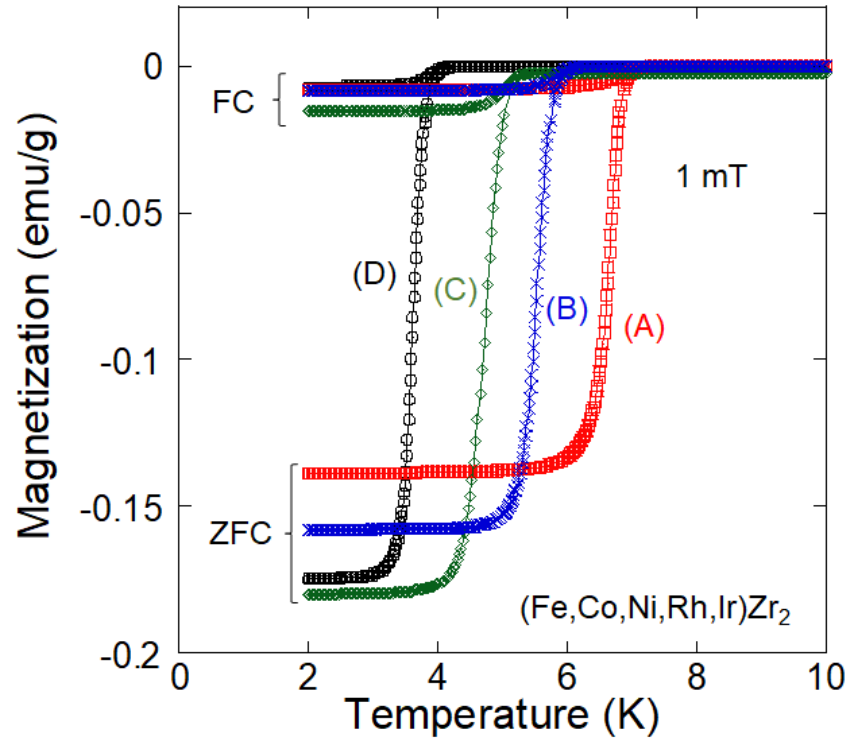


Fig. 4. Temperature dependences of magnetization for TrZr_2 samples (A)–(D).

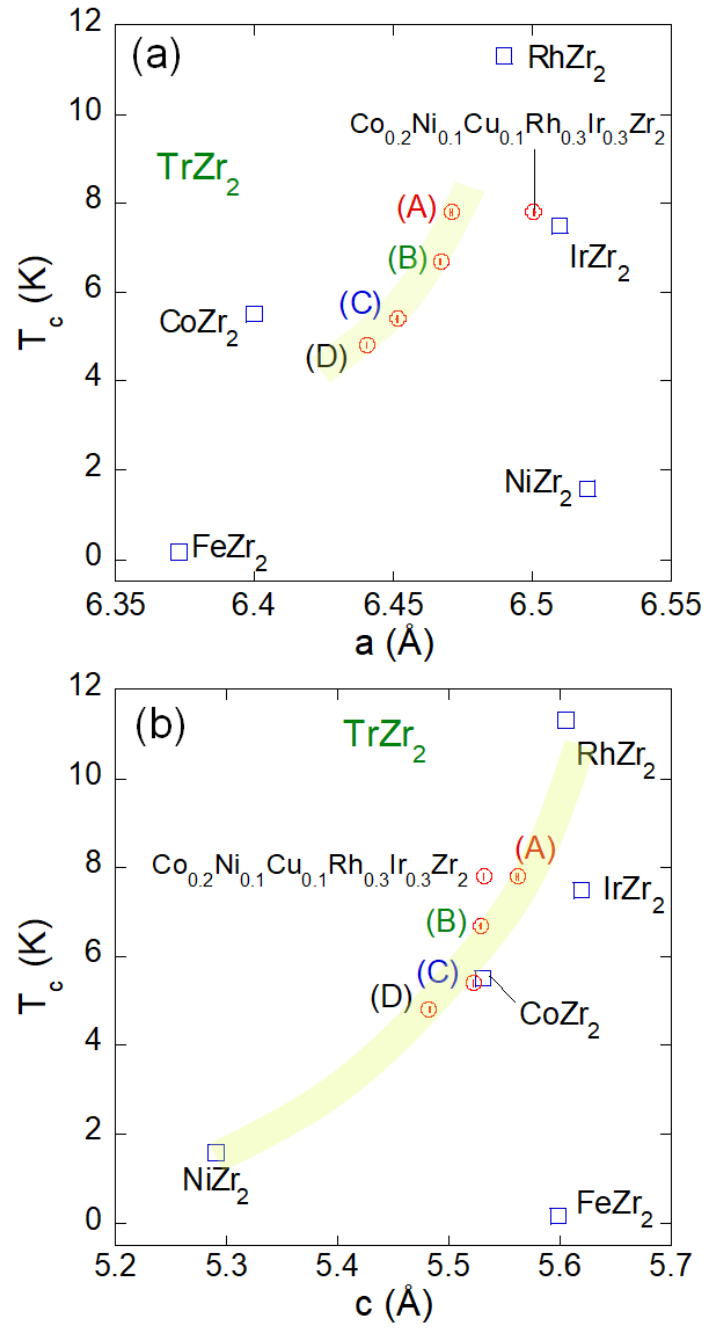


Fig. 5. Lattice constant dependences of T_c for $TrZr_2$. Data of T_c and lattice constants were taken from Refs. 21, 22, 28-31.

REFERENCES

1. Fagaly RL (2006) Superconducting quantum interference device instruments and applications. *Rev. Sci, Instru.* 77:101101(1-45).
2. Koželj P, Vrtnik S, Jelen A et al (2014) Discovery of a Superconducting High-Entropy Alloy. *Phys, Rev. Lett.* 113:107001(1-5).
3. Sun L, Cava RJ (2019) High-entropy alloy superconductors: Status, opportunities, and challenges. *Phys. Rev. Mater.* 3:090301(1-10).
4. Marik S, Varghese M. Sajilesh KP, Singh D, Singh RP (2019) Superconductivity in a new hexagonal high-entropy alloy. *Phys. Rev. Mater.* 3:060602(1-6).
5. Vrtnik S, Koželj P, Meden A, Maiti S, Steurer W, Feuerbacher M, Dolinsek J (2017) Superconductivity in thermally annealed Ta-Nb-Hf-Zr-Ti high-entropy alloys. *J. Alloy Compound* 695:3530-3540.
6. Stolze K, Cevallos FA, Kong T, Cava RJ (2018) High-entropy alloy superconductors on an α -Mn lattice. *J. Mater. Chem. C* 6:10441-10449.
7. Yuan Y, Wu Y, Luo H et al (2018) Superconducting $\text{Ti}_{15}\text{Zr}_{15}\text{Nb}_{35}\text{Ta}_{35}$ High-Entropy Alloy With Intermediate Electron-Phonon Coupling. *Front. Mater.* 5:72(1-6).
8. Ishizu N, Kitagawa J (2019) New high-entropy alloy superconductor $\text{Hf}_{21}\text{Nb}_{25}\text{Ti}_{15}\text{V}_{15}\text{Zr}_{24}$. *Results in Phys.* 13:102275(1-2).
9. von Rohr FO, Cava RJ (2018) Isoelectronic substitutions and aluminium alloying in the Ta-Nb-Hf-Zr-Ti high-entropy alloy superconductor. *Phys. Rev. Mater.* 2:034801(1-7).
10. Stolze K, Tao J, von Rohr FO, Kong T, Cava RJ (2018) Sc-Zr-Nb-Rh-Pd and Sc-Zr-Nb-Ta-Rh-Pd High-Entropy Alloy Superconductors on a CsCl-Type Lattice. *Chem. Mater.* 30:906-914.
11. Guo J, Wang H, von Rohr FO et al (2017) Robust zero resistance in a superconducting high-entropy alloy at pressures up to 190 GPa. *Proc. Natl. Acad. Sci. U.S.A.* 114:13144-13147.
12. Yeh JW, Chen SK, Lin SJ et al (2004) Nanostructured High-Entropy Alloys with Multiple Principal Elements: Novel Alloy Design Concepts and Outcomes. *Adv. Eng. Mater.* 6:299-303.

13. Tsai MH, Yeh JW (2014) High-Entropy Alloys: A Critical Review. *Mater. Res. Lett.* 2:107–123.
14. Sogabe R, Goto Y, Mizuguchi Y (2018) Superconductivity in $\text{REO}_{0.5}\text{F}_{0.5}\text{BiS}_2$ with high-entropy-alloy-type blocking layers. *Appl. Phys. Express* 11:053102(1–5).
15. Shukunami Y, Yamashita A, Goto Y, Mizuguchi Y (2020) Synthesis of RE123 high-Tc superconductors with a high-entropy-alloy-type RE site. *Physica C* 572:1353623(1–5).
16. Mizuguchi Y (2019) Superconductivity in High-Entropy-Alloy Telluride AgInSnPbBiTe_5 . *J. Phys. Soc. Jpn.* 88:124708(1–5).
17. Kasem MR, Hoshi K, Jha R et al (2020) Superconducting properties of high-entropy-alloy tellurides M-Te (M: Ag, In, Cd, Sn, Sb, Pb, Bi) with a NaCl-type structure. *Appl. Phys. Express* 13:033001(1–4).
18. Yamashita A, Jha R, Goto Y, Matsuda TD, Aoki Y, Mizuguchi Y (2020) An efficient way of increasing the total entropy of mixing in high-entropy-alloy compounds: a case of NaCl-type $(\text{Ag, In, Pb, Bi})\text{Te}_{1-x}\text{Se}_x$ ($x = 0.0, 0.25, 0.5$) superconductors. *Dalton Trans.* 49:9118–9122.
19. Fujita Y, Kinami K, Hanada Y et al (2020) Growth and Characterization of ROBiS_2 High-Entropy Superconducting Single Crystals. *ACS Omega* 5:16819–16825.
20. Sogabe R, Goto Y, Abe T, Moriyoshi C, Kuroiwa Y, Miura A, Tadanaga K, Mizuguchi Y (2019) Improvement of superconducting properties by high mixing entropy at blocking layers in BiS_2 -based superconductor $\text{REO}_{0.5}\text{F}_{0.5}\text{BiS}_2$. *Solid State Commun.* 295:43–49.
21. Mizuguchi Y, Matsuda TD (2020) Superconductivity in CuAl_2 -type $\text{Co}_{0.2}\text{Ni}_{0.1}\text{Cu}_{0.1}\text{Rh}_{0.3}\text{Ir}_{0.3}\text{Zr}_2$ with a high-entropy-alloy transition metal site. *arXiv:* 2009.07548.

22. Fisk Z, Viswanathan R, Webb GW (1974) THE RELATION BETWEEN NORMAL STATE PROPERTIES AND T_c FOR SOME Zr_2X COMPOUNDS. Solid State Commun. 15:1797–1799.
23. Matthias BT, Corenzwit E (1955) Superconductivity of Zirconium Alloys. Phys. Rev. 100:626–627.
24. Teruya A, Kakihana M, Takeuchi T et al (2016) Superconducting and Fermi Surface Properties of Single Crystal Zr_2Co . J. Phys. Soc. Jpn. 85:034706(1–10).
25. Bonhomme F, Yvon K, Zolliker M (1993) Tetragonal Zr_2CoD_5 with filled Al_2Cu -type structure and ordered deuterium distribution. J. Alloys Compd. 199:129-132.
26. Sefat AS, Jin R, McGuire MA, Sales BC, Singh DJ, Mandrus D (2008) Superconductivity at 22 K in Co-Doped $BaFe_2As_2$ Crystals. Phys. Rev. Lett. 101:117004(1-4).
27. Mizuguchi Y, Tomioka F, Tsuda S, Yamaguchi T, Takano Y (2009) Substitution Effects on FeSe Superconductor. J. Phys. Soc. Jpn. 78:074712 (1-5).
28. Raj P, Suryanarayana P, Sathyamoorthy A, Shashikala K, Iyer RM (1992) Zr_2FeH_x system hydrided at low temperatures: structural aspects by Mössbauer and x-ray diffraction studies. J. Alloy Compounds 178:393-401.
29. Yamaya K, Sambongi T, Mitsui T (1970) Superconductivity and Magnetic Susceptibility of Zr_2Co - Zr_2Ni System. J. Phys. Soc. Jpn. 29:879-884.
30. Jorda JL, Graf T, Schellenberg L, Muller J, Cenzual K, Gachon JC, Hertz J (1988) Phase relations, thermochemistry and superconductivity in the Zr-Rh system. J. Less Common Metals 136:313-328.
31. AtomWork, NIMS database (<http://crystdb.nims.go.jp/>)
32. Prajapat CL, Chattaraj D, Mishra R, Singh MR, Mishra PK, Ravikumar G (2016) Magnetic properties of $FeZr_2$ and Fe_2Zr intermetallic compounds. AIP Conf. Proc. 1731:130015.

Supporting information

Synthesis of high-entropy-alloy-type superconductors (Fe,Co,Ni,Rh,Ir)Zr₂ with tunable transition temperature

Md. Riad Kasem¹, Aichi Yamashita¹, Yosuke Goto¹, Tatsuma D. Matsuda¹, Yoshikazu

Mizuguchi^{1*}

2. Department of Physics, Tokyo Metropolitan University, 1-1, Minami-osawa, Hachioji, 192-0397.

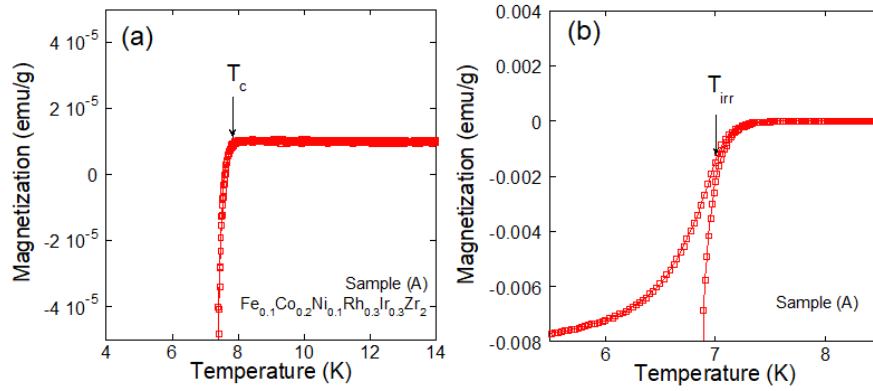


Fig. S1. Estimation for T_c and T_{irr} from the temperature dependence of magnetization for sample (A).